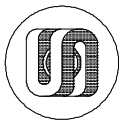

IHEP, Protvino, Russia

Experimental Study and Finite Element Analysis of the Heat Diffusion Problem for ATLAS MDT Chamber.

L.Baliev, A.Borisov, A. Kojine

Institute for High Energy Physics
Protvino,142248, Moscow region, Russia

Abstract.

The experimental study of the heat diffusion problem with using of the small MDT prototype and Finite Element Analysis (FEA) of this prototype and BIL Chamber's Multilayer is presented. The Finite Element program used in this analysis was ANSYS4.4.

All questions and notes address to: **BALIEV@MX.IHEP.SU or KOZHIN@MX.IHEP.SU.**

1. Introduction.

This paper describes the experimental and analysis parts of a heat diffusion problem study for the MDT Chamber with small prototype using. The reason of this study is the results of the BIL Muon Chamber design concept analysis presented in the references 1 and 2.

The goals of this work were:

- study of the heating influence of the front end electronics on the temperature distribution into the Chamber;

- experimental redetermination of the finite element model (FEM) parameters, such as air thermal conductivity between drift tubes (λ) and convection coefficient of the upper and lower layers (α). This redetermination is necessary to make thermal FEA of the BIL Muon Chamber more correct.

2. Experimental part.

2.1. Setup.

The measurements were performed for a prototype consisting of 17 Al tubes with 30mm outer diameter, 0.5mm wall thickness and 85cm length, bounded together with distance between walls 0.1mm. The prototype was placed inside cardboard box (Figure 1) to prevent an air side flow. Right and left sides of the prototype were shielded by foam plates, but some

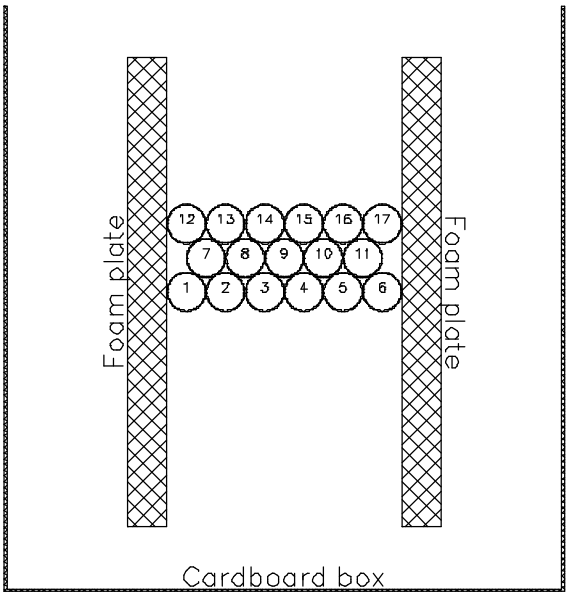

Figure 1: Setup for test of drift tubes heating by front end electronics.

measurements were done without them. The plates reduce heat flow near prototype sides for better approach to the chamber with larger width. The tube ends are closed by foam end plugs (Figure 2). We tested two cases of heat sources: one inside tubes and another at a board placed near the end of tube. Resistor (2W 200Ohm) attached to the left end plug simulates heat source inside tube, for example, preamplifier inside Faraday-cup attached to the tube. Figure 3 shows cross section of the prototype heated end when the heat source is placed at the board. It consists of 18 2W resistors distributed on the board. The board was closed by a box made of 1.5mm Al.

The box was attached to tubes. The width of contact surface of the box with an external tube of the prototype is about of tube diameter. For corner tubes of the prototype the contact width with the box is doubled. Length of the contact (D_c in Figure 3) could be changed, but the contact surface was not perfect. The gap between tube and the box could be up to 1.5mm. We used two boxes. One was closed. Up and down sides of the second box were drilled. Holes' diameter is 7mm, they covered about 23% of the box side.

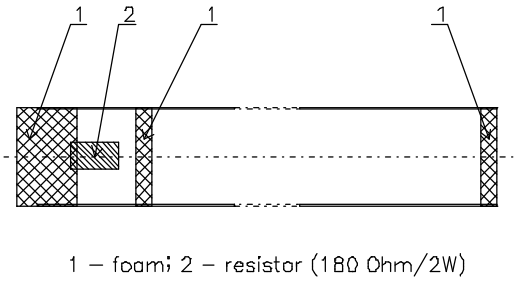

Figure 2: Cross-section of tube.

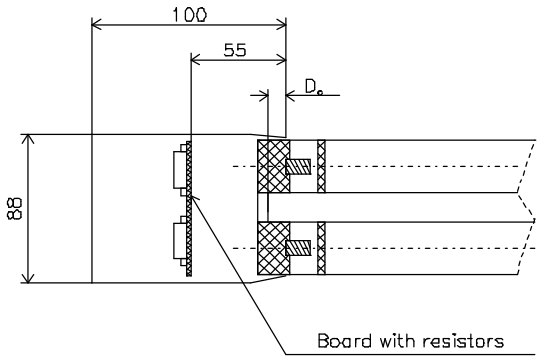

Figure 3: Box with heated board.

Temperature of tubes was measured by thermoresistor that was attached to the wall of a tube inside it. Calibration curve of the resistor is given in Figure 4. For calibration thermoresistor

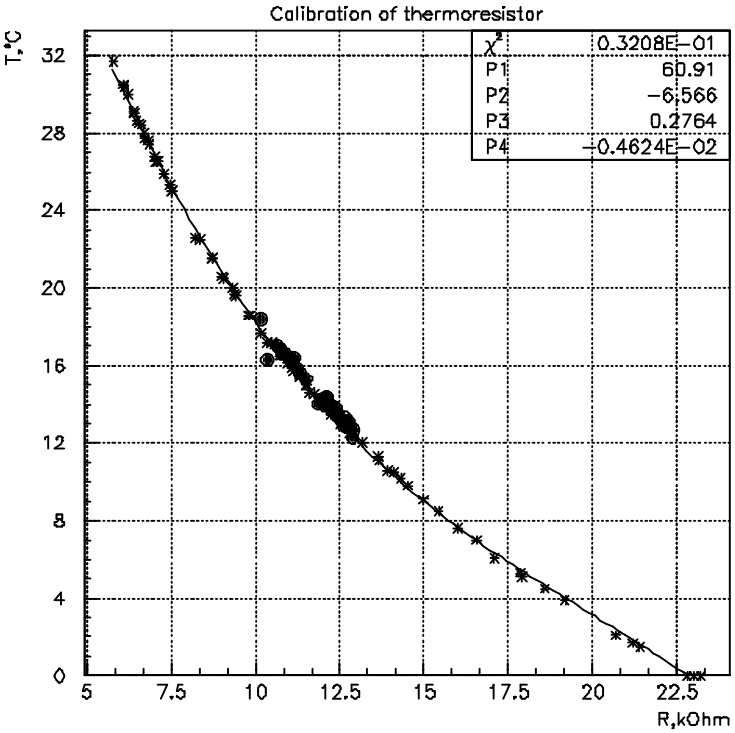

Figure 4: Calibration of the temperature sensor: asterisk -- calibration points, full cycles -- points during measurements.

was attached to internal surface of Al tube which was placed in tank with water the temperature of which was measured by mercury thermometer with resolution of 0.1°C (asterisks in Figure 4). Full cycles denote points measured in Al tubes of the prototype during test before heating, when air temperature was measured by the mercury thermometer. These points were not used to fit.

2.2. Results with heat source inside tube.

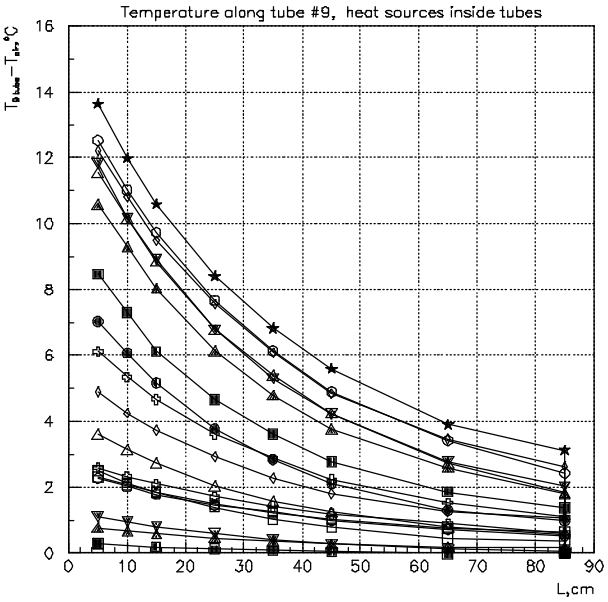

Figure 5: Temperature of tube 9 versus length for different powers. For definition of marker type see Figure 6.

The first measurements were done with heat sources inside tubes. We measured temperature along tube #9 and distribution of the temperature across drift tubes at distance 5cm from hot ends. Measurements were performed in 3 or more hours after switch on power supply heating the tubes. Further when we shall tell about tube temperature it will mean the difference between temperature of tube and air temperature. Figure 5 shows temperature in tube 9 versus length from heated end for different powers inside tube. To recognize value of the power one needs to see in Figure 6 where the hot end temperature is shown as a function of the power. Marker type of Figure 6 corresponds to one in Figure 5. Asterisks in Figure 6 denote difference of temperature between heated

and cold tube ends. Figure7 gives tube cold end temperature versus power. The results given in Figure 5-7 were obtained with one foam plate at right side of the prototype (Figure 1). Line fit of the results in Figure 5 gives temperature of heat end as 0.014±0.0008°C*P(mW/tube), where P is the tube heating power.

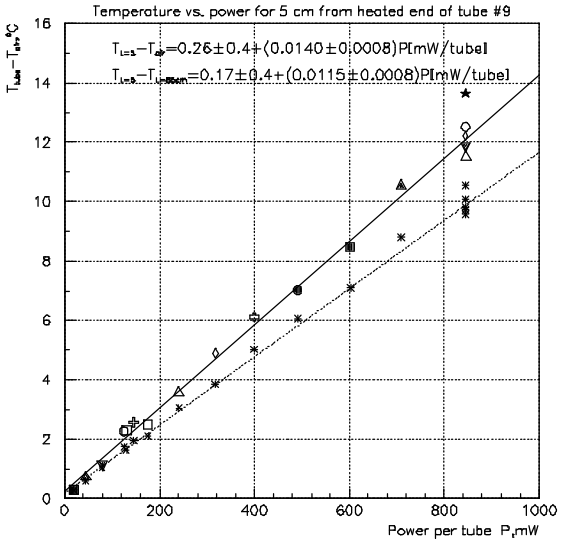

Figure 6: Temperature of the heated end as a function of power. Asterisks' difference temperature between hot and cold ends.

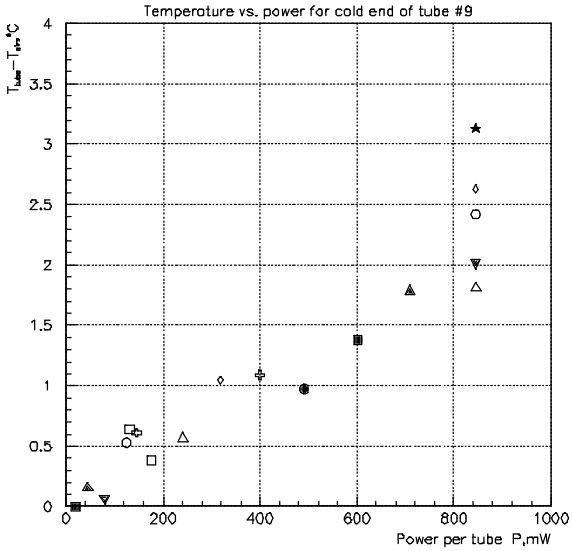

Figure 7: Temperature of cold end versus power.

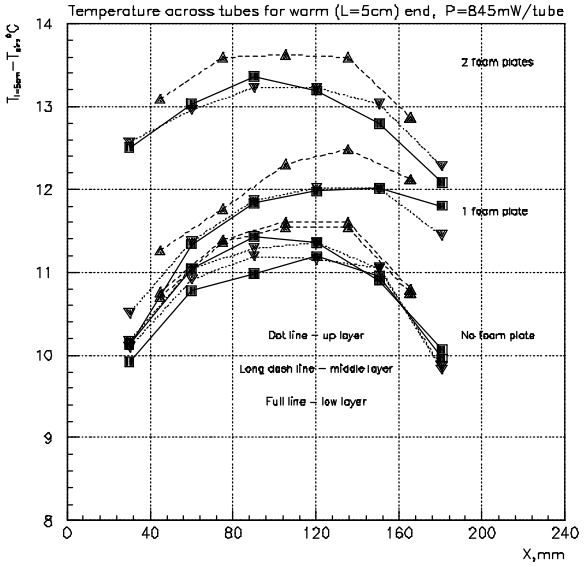

Figure 8: Distribution of temperature across tubes for 845mW/tube power inside tube at L=5cm from hot end.

Distribution of temperature across drift tubes at distance 5cm from heated end is presented in Figure 8 for 845 mW/tube power and for 3 cases: without foam plates (two sets of measurements);1 foam plate and 2 foam plates at sides of the prototype.

2.3. Results with heat source on the board.

For the 1st case when the box around the board was not drilled we performed limited number of measurements. We tested only two values of power supposing that temperature of the tube is linear function of power. Previous results with heat source inside tube (Figure 6) prove it. The measurements were done with 2 foam plates.

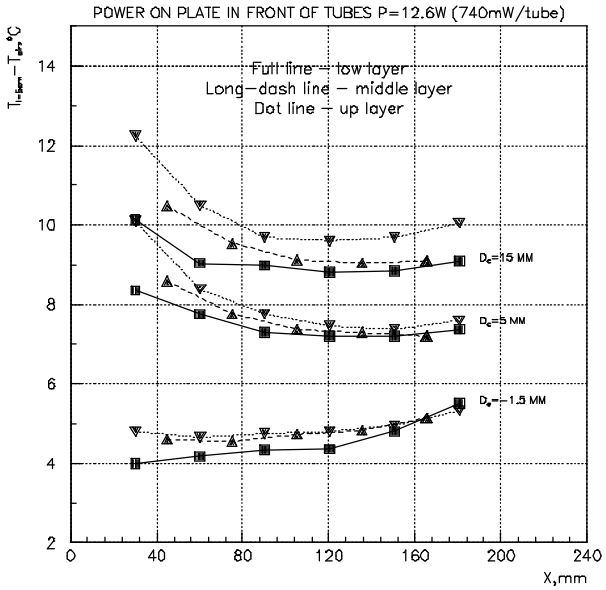

Figure 9: Distribution of temperature across tubes at L=5cm from hot end. Power is 740mW/tube at common board.

Distribution of temperature across tubes at distance 5cm from heated end is shown in Figure 9 for three lengths of contact between the box around the heat board and tubes. Value of the length is given near corresponding family of curves. Negative value means that there is not a contact between tubes and the box that is attached to foam end plugs only. Increasing the temperature at edges is caused by about doubled contact surface width for corner tubes.

Distribution of the temperature along tube 9 is given in Figure 10 for different contact conditions of the box with tube and two values of power. Marker type definition can be understood from Figure 11. Line dependence of tube temperature versus board power gives us 0.006, 0.009 and 0.012°C*P(mW/tube) for D_c equal to --1.5, 5 and 15mm, accordingly.

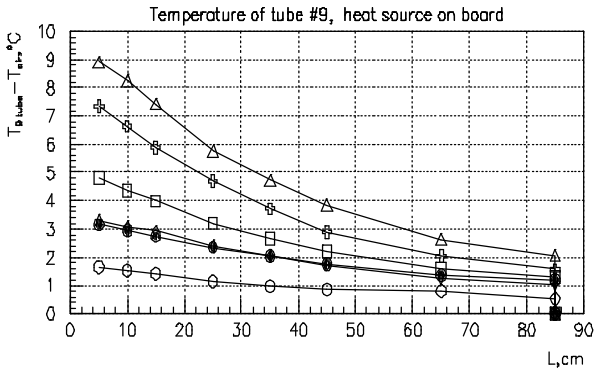

Figure 10: Temperature of tube #9 versus length for different powers at common board. Box was not drilled. For definition of marker type see Figure 11.

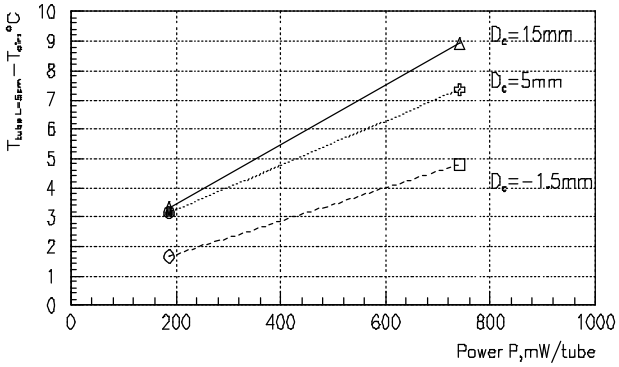

Figure 11: Temperature of heated end as a function of power at common board with undrilled box.

For the drilled box we measured temperature in tube 9 versus power more carefully. Dependences of tube 9 temperature as a function of power is shown in Figure 12 for distance 5cm from heated end. Values of the contact length are given near curves which are the 2nd order polynomial fit.

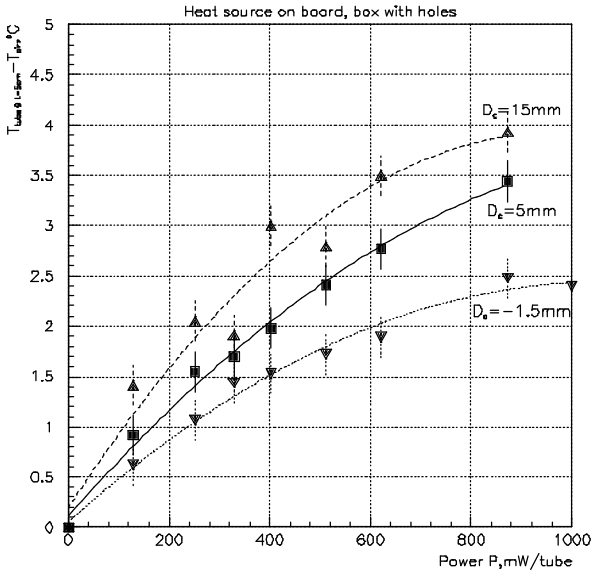

Figure 12: Temperature of heated end as a function of power at common board with drilled box, holes' diameter is 7mm, surface of holes is 23%.

2.4. Discussion of the measurement results.

We should like to emphasize that our measurement is zero approach to the problem. However now we have several digits that can be used for estimations.

When heat source is placed inside tube, e.g. preamplifier inside end plug, signal end of tubes will be heated with respect air as 0.014°C*P(mW/tube), where P is power. The value was obtained for short (85cm) tubes. Increasing of the tube length will decrease the end temperature by about 20%, but we suppose that 4-layers chamber will have temperature some larger as compare to 3-layers one. So, we conserve our estimation.

It is detected temperature difference between tube layers. The value is about 0.3-0.4°C for heated tube ends for power of 845mW/tube.

Estimation of temperature for heat source at board, e.g. common board with amplifiers like "hedgehog", is 0.006-0.012°C*P(mW/tube). The value is dependent of shielding box thermal contact with the end of MDT chamber. For the box with drilled surface the tube's temperature is about two times less as compare to the closed box. We think that the temperature can be increased due to pins between the board and end plugs. It has to be tested with real construction of the MDT chamber.

3. Analysis part.

3.1. Finite Element Model.

2-D (X-Y axes) FEM was used to simulate prototype (Figure 13) and BIL Chamber's multilayer (Figure 14).

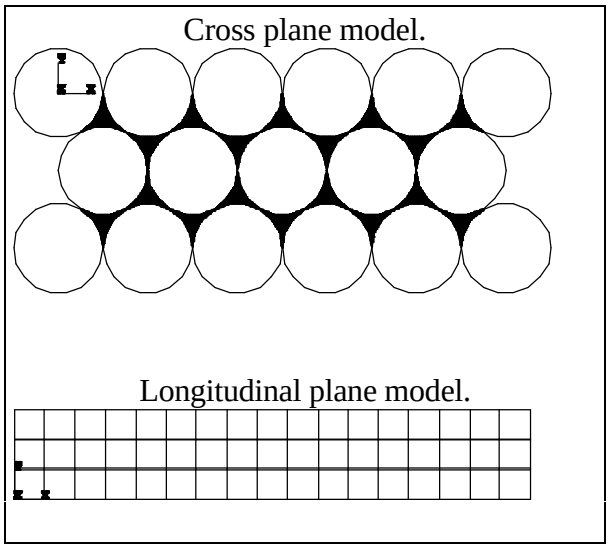

Figure 13: Small prototype FEM.

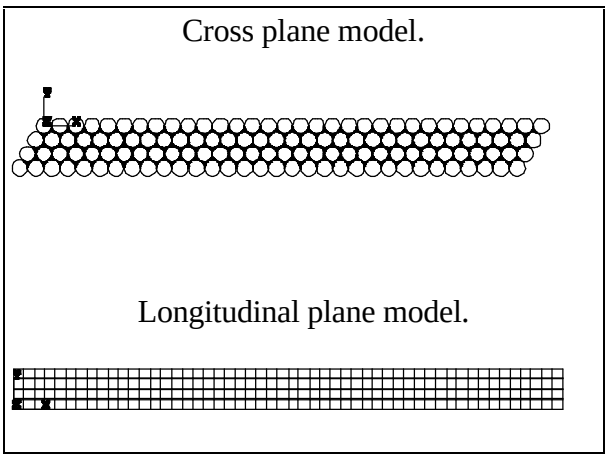

Figure 14: MDT Chamber's multilayer FEM.

The element types used were:

- STIF32 (2 nodes Thermal Bar) to model the drift tube's cross section;
- STIF33 (2 nodes Thermal Bar) to model the drift tub's longitudinal section and air between tubes in longitudinal model:
- STIF34 (2 node Convection Link) to model convection between outside surface of the prototype or Chamber's multilayer and environmental air;
- STIF55 (4 node Isoparametric Thermal Solid) to model air space between drift tubes.

3.2. Material properties.

Two materials types were used in FEM - Aluminium alloy for the drift tubes and air in the space between drift tubes. The material properties for the different model elements are shown in Table 1.

Table 1.

	Drift tubes	Air	Up surface	Low surface	Lateral surface
Thermal conductivity (W/m∗°C)	209.3	$\lambda_x = 0.026$ $\lambda_y = 0.154$	-	-	-
Heat capacity (J/kg∗°C)	880	1000	-	-	
Mass density (kg/m^3)	2630	1.29	-	-	-
Convection coefficient prototype (W/m^2 ∗°C)	-	-	2.17	1.77	2.4
Convection coefficient multilayer (W/m^2 ∗°C)	-	-	1.42	1.16	2.24

3.3. Loading.

The heat source (845 mW) was applied to one end of each drift tube.

3.4. Analysis plan.

The analysis was made in the following sequence:

- The several calculations were carried out for the cross plane of the prototype[2] (Figure 13). As result air thermal conductivity coefficient and convection one were matched so that cross plane temperature distribution obtained by calculations became the same as one for the prototype;

- The calculations for the longitudinal plane of the prototype (Figure 13) with using of previous calculation results were carried out. By result the temperature distribution along the drift tubes was obtained. Agreement of this distribution with measured one was a criterion of the FEM correctness;

- The calculations for the cross plane and longitudinal one of the Chamber's multilayer (Figure14) with utilizing of the calculation results for the prototype were carried out;

[1] Standard value of the air thermal conductivity is equal to 0.026, but convection's presence makes it value equal to 0.154.
[2] All calculations were made for prototype without foam plates.

- The estimations of the Chamber's sag under temperature gradient influence were carried out.

3.5. Calculation results.

We came to the conclusion that the most good agreement between calculation and experimental results (Figures 14,15) can be obtained when FEM parameters will have following values:

$\lambda_x = \lambda_s$;

$\lambda_y = 6 \cdot \lambda_s$;

$\alpha_{lat} = 2.4(\mathrm{W} / \mathrm{m}^2 \cdot {}^\circ C)$;

$\alpha_{up} = 1.1 \cdot \alpha_{lat}$;

$\alpha_{low} = 0.9 \cdot \alpha_{lat}$;

Where:

λ_x is air thermal conductivity between drift tubes in X direction;

λ_y is air thermal conductivity between drift tubes in Y direction;

$\lambda_s = 0.026(W / m \cdot {}^\circ C)$ is standard value of the air thermal conductivity;

α_{lat} is convection coefficient of the lateral layer;

α_{up} is convection coefficient of the upper layer;

α_{low} is convection coefficient of the lower layer.

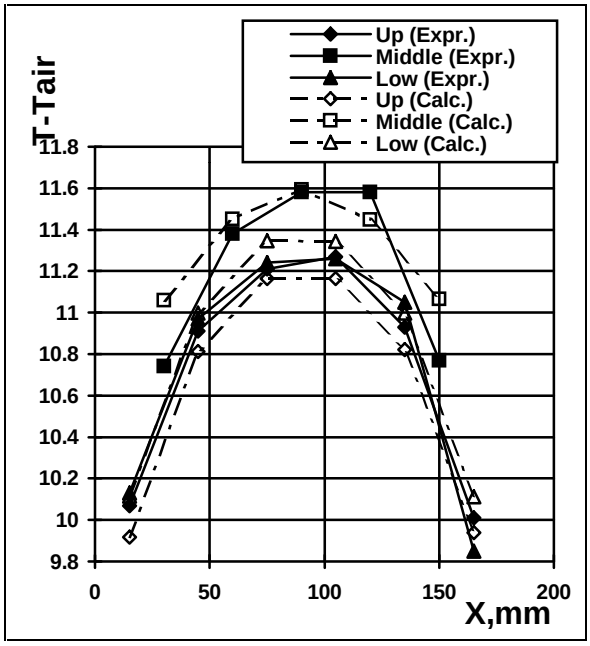

Figure 15: Distribution of temperature across tubes obtained by measurement and calculations.

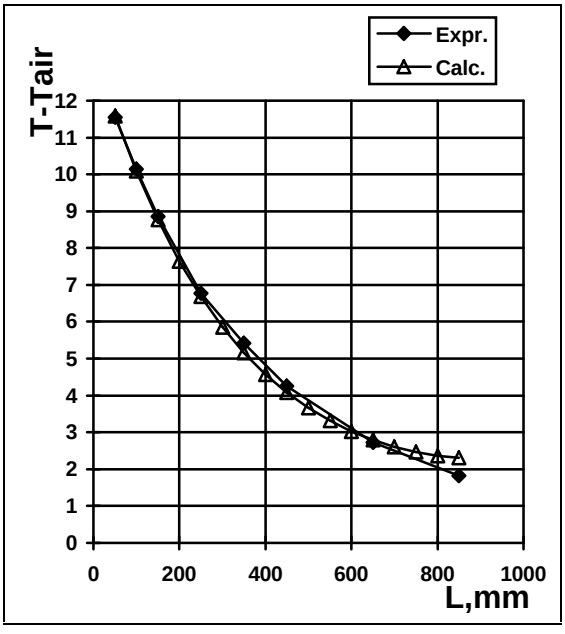

Figure 16: Temperature along tube #9 obtained by measurement and calculations.

The results of calculations for BIL Chamber's multilayer are shown in Figure 17 and 18. The temperature distribution given in Figure 18 was carried out for multilayer cross plane center line.

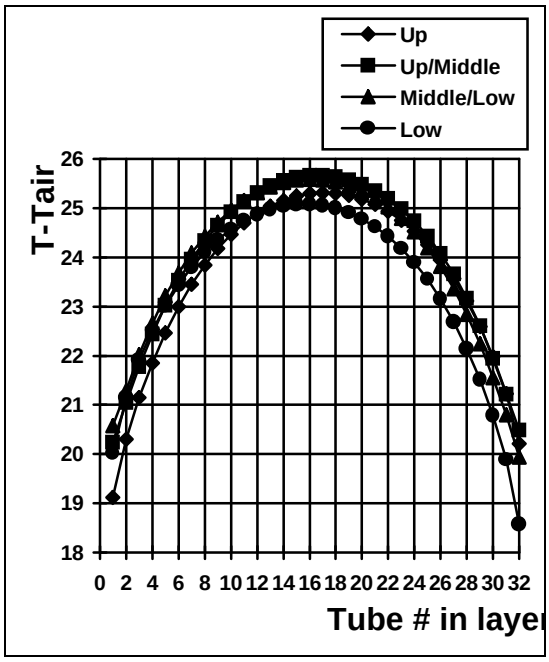

Figure 17: Distribution of temperature across tubes for BIL Chamber's multilayer.

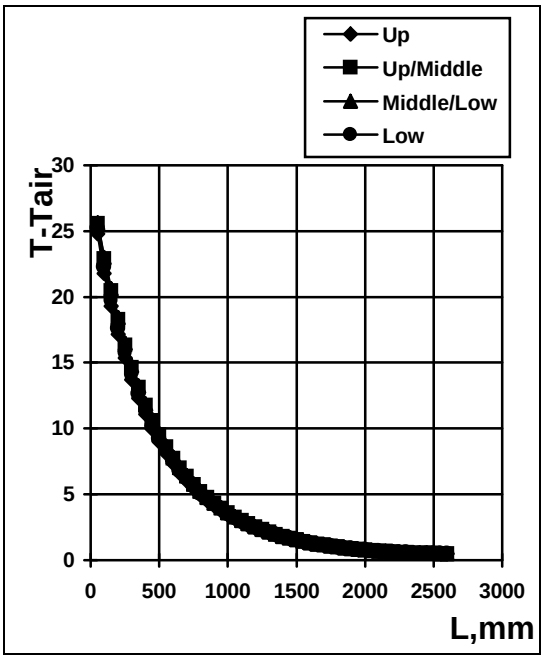

Figure 18: Temperature distribution along tube #16 for each layer.

The minimal Chamber's sag under normal to the Chamber's plane temperature gradient influence was estimated as equal to 90μm[3] (for heat source equal to 845 mW per tube).

3.6. Discussion of the calculations results.

The change-over from prototype FEM to Chamber's multilayer FEM leads to the pronounced increment of the maximal drift tubes' temperature (from 11.6°C to 25.6°C).

The temperature gradient normal to the Chamber's plane is quite big (from 0.01...0.53°C between neigbouring layers for central area of the Chamber to 0.27...1.37°C for outlying area) and Chamber's sag under this gradient influence can exceed allowable value.

The temperature gradient along of the drift tubes is also big, that leads to the different value of the thermal expansion for different Chamber's end (according to our estimation this difference can reache 560μm).

[3] Allowable value is 110±25μm.

The temperature gradient in the Chamber's plane, but across drift tubes is large (up to 6.51°C between central tube and outlying one) that can lead to the pronounced deformations in Chamber's plane. Moreover, because of the Chamber's multilayer cross section is asymmetrical (Figure 13), the temperature distribution in drift tubes' layer is asymmetrical too (Figure17). It can lead to a warping of the Chamber's multilayer.

It looks as if the problem of the heating influence to the Chamber's deformation is quite serious problem and requires further study. However it is clear already now, that there is necessity to find some technical solutions to provide uniform temperature in the Chamber.

4. Conclusions.

- Chamber's temperature deformations are a real problem, which must be studied thoroughly;
- Temperature gradient in the Chamber leads to complex three-dimensional deformations;
- Temperature deformations value can exceed its allowable value.

References:

1. "Initial Finite Element Analysis of a Barrel Inner Large Muon Chamber for ATLAS. Part1.", L.Baliev, IHEP, Russia, November 11, 1995.

2. "Initial Finite Element Analysis of a Barrel Inner Large Muon Chamber for ATLAS. Part2.", L.Baliev, IHEP, Russia, November 11, 1995.